XL CILAMCE
IBERO-LATIN AMERICAN
CONGRESS ON
COMPUTATIONAL
METHODS IN
ENGINEERING

NOVEMBER
11-14, 2019
Praiamar Natal Hotel & Convention
Natal, RN-BRAZIL

SHIFTED BOUNDARY METHOD FOR POISSON PROBLEMS IN LIBMESH

Vinicius da C. Reis
viniciusreis@coc.ufrj.br
Alvaro L.G.A Coutinho
alvaro@nacad.ufrj.br
Department of Civil Engineering COPPE/Federal University of Rio de Janeiro
Av. Athos da Silveira Ramos, 149, 21941-909, Rio de Janeiro, Brazil

Abstract.

The embedded finite element method is one approach to diminish the mesh generation burden in finite element analysis. It consists of dealing with a description of a boundary that does not necessarily match the problem's physical boundary. It can potentially shrink the workflow giving the opportunity of immediately inputting a CAD geometry or tomographic image into a simulation, without necessarily using isogeometric elements or performing substantial preprocessing. This work presents an implementation of the recently proposed embedded formulation for Poisson problems in the general purpose library libMesh. In the formulation, the boundary condition is shifted and enforced weakly by a Nitsche approach, and then referred as surrogated boundary. This is accomplished provided the surrogate boundary is close enough to the physical boundary so a Taylor expansion can be used to describe the chopped off region. This approach provides a significant computational relief compared to the alternative selected point integration, especially when dealing with complex domains where the total point-locating operations' cost can be significantly high. Moreover, computational experiments indicates that second order convergence can achieved.

Keywords: Shifted boundary, Embedded method, Weak boundary conditions, libMesh, Finite element method

1 Introduction

The unfitted methods is a broad term that encompasses a collection of numerical methods' formulations that are dedicated to solve problems where the mapped geometry of a physical body does not match the contour of the grid or mesh put in place to represent it. Though having its main application in fluid mechanics and fluid structure interaction problems, they are also applicable to other physics.

They are suitable to be used in situations where the mesh generation is such a burden that might even render a problem unsolvable. On the other hand it has been reported [Boggs et al.] that most of the time spent on simulation is on geometry manipulation or mesh generation. As an attempt to cut the intermediate steps between a model conception and its simulation, by adopting B-splines, NURBS or T-splines as base functions, traditionally used as CAD surfaces, the isogeometric formulations is then proposed[2]. An equivalent result might be achieved by using the same functions merely as geometric description in a unfitted method. Regardless on the motivation, whenever geometric manipulation or the mesh generation becomes an issue, either for the manual labor required or the computational cost, the unfitted methods should be considered.

Although frequently used interchangeably, the terms immersed and embedded can be distinguished, separating the unfitted methods in two mains categories. This distinction is made by Main and Scovazzi [3, 4] grouping as immersed the set of formulations that prescribes the discretization of a problem in the entirety of a mesh, that usually is defined as a regular region of the cartesian space, bounding the domain under evaluation and its defining boundary. Conversely the embedded formulations are the ones that removes the elements or cells that are not part of the domain, entirely or, depending on the formulation, partially.

Among immersed formulation is the pioneer work of Peskin [5] and the level-set methods [6]. On these formulations the enforcement of the boundary condition is done by applying an equivalent force field that can be interpreted as a penalty function.

Within the embedded formulations are the methods derived from the XFEM [7] formulation with boundary condition enforced by Nitsche's method [8]. On this approach, by enriching the approximation space by mean of a discontinuous function it is possible to correctly represent the boundary. The conjunction of the two techniques is examined by Hansbo and Hansbo [9] for a diffusion problem in a discontinuous domain. One of the challenges imposed by this approach is the complexity of correctly detecting the boundary interception in a element.

Still on the embedded category, an interesting approach, designated as Finite Cell Method, is developed for solid mechanics [10] and turbulent flow [11] problems. In this approach the boundary condition representation is achieved by removing elements that lies outside of the geometry under evaluation and an adaptive integration scheme is adopted on the elements crossed by the boundary. The downside of this technique is the point by point location evaluation that can be computationally expensive depending on the size of the problem, the number of integration points used and the complexity of the geometry. In its implementation a ray trace algorithm is used, but it is not necessarily the only solution. A review of this method is done by Schillinger [12].

Finally in the embedded set of formulations, grouped in the approximate domain methods, is the Shifted Boundary Method. The boundary condition is shifted and enforced weakly by Nitsche approach, and then referred as surrogated boundary. Its full development and analysis can be found on its original publication [3], here being reported just its final statement. The Nitsche formulation is also implemented as a reference solution and is used to evaluate the quality of the shifted boundary formulation. The surrogate boundary has to be close enough to the true boundary, so that a Taylor expansion can be used to describe the chopped off region.

The implementation is done in the framework libMesh [14] and takes advantage of the subdomain functionality, after geometric evaluations, to segregate the elements crossed by the true boundary, its neighbors inside the domain, composing the surrogate boundary, and the inner and outer elements. The two geometric shapes used to compose the evaluated geometries are circles and spheres.

The remainder of this paper is organized as follows. The next section presents briefly the shifted boundary method. Section 3 shows the obtained results and the observed convergence for two and three-dimensional problems. The paper ends with a summary of our main findings.

2 The shifted boundary method

The model evaluated is the classical Poisson problem with Dirichlet boundary condition: find the solution $u \in C^2(\Omega)$ such that

$$\begin{aligned} -\triangle u &= f, &\quad& \text{on} \quad \Omega \\ u &= u_D, &\quad& \text{on} \quad \Gamma_D = \partial\Omega. \end{aligned} \tag{1}$$

The shifted boundary method starts by defining a surrogate domain $\widetilde{\Omega}$ bounded by $\widetilde{\Gamma}$, the surrogate boundary. The relation $(\widetilde{\Omega} \cup \widetilde{\Gamma}) \subset \Omega$ holds and $\mathbf{d}$ is the distance vector between the surrogate and the true boundary. Any surrogate boundary related quantity is then annotated with an over tild as ilustraded in figure 1.

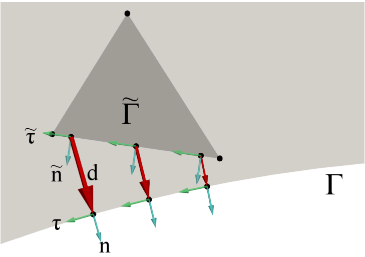

Figure 1. True and surrogate boundary with normal, tangent and distance vector.

The definition of a map function

$$\begin{aligned} \mathbf{M} :& \widetilde{\Gamma} \to \Gamma \\ & \widetilde{x} \to x \end{aligned} \tag{2}$$

from the surrogate boundary to the real boundary, is necessary so that any quantity can be shifted from one to the other. The shifting of an arbitrary function ψ can then be defined as

$$\overline{\psi}(\widetilde{x}) \equiv \psi(\mathbf{M}(\widetilde{x})). \tag{3}$$

For the simple geometries evaluated in this work the closest distance is the natural mapping choice, and, as a beneficial consequence, the distance vector is aligned with the mapped true normal.

The shifted unitary normal vector is defined as

$$\overline{\mathbf{n}}(\widetilde{\mathbf{x}}) \equiv \mathbf{n}(\mathbf{M}(\widetilde{\mathbf{x}})). \tag{4}$$

The derivative of an arbitrary function ψ on the surrogate boundary, projected onto the shifted normal is stated as:

$$\psi_{,\overline{\mathbf{n}}}(\widetilde{\mathbf{x}}) = \nabla\psi(\widetilde{\mathbf{x}}) \cdot \overline{\mathbf{n}}(\widetilde{\mathbf{x}}) = \nabla\psi(\widetilde{\mathbf{x}}) \cdot \mathbf{n}(\mathbf{M}(\widetilde{\mathbf{x}})). \tag{5}$$

Building upon the previews definition it is then possible to evaluate the Taylor expansion centered at the surrogate boundary, i.e. for $\widetilde{\mathbf{x}} \in \widetilde{\Gamma}$ as

$$0 = u\left(\widetilde{\mathbf{x}}\right) + \nabla u\left(\widetilde{\mathbf{x}}\right) \cdot \left(\mathbf{x} - \widetilde{\mathbf{x}}\right) - \overline{u}_D\left(\widetilde{\mathbf{x}}\right) + O\left(||\mathbf{x} - \widetilde{\mathbf{x}}||^2\right) \tag{6}$$

Finally as a preliminary definition, the inner product $L^2\left(\omega\right)$ for $\omega \subset \Omega$ and $\gamma \subset \Gamma$ is defined as:

$$\left(v, w\right)_\omega = \int_\omega vw \, d\omega \qquad \text{and} \qquad \left(\mathbf{v}, \mathbf{w}\right)_\omega = \int_\omega \mathbf{v} \cdot \mathbf{w} \, d\omega \tag{7}$$

for both $\Omega \subset \mathbb{R}$ and $\Omega \subset \mathbb{R}^{n_d}$ respectively, where n_d is the space dimension. Also functionals on γ are defined:

$$\left\langle v, w\right\rangle_\gamma = \int_\gamma vw \, d\gamma \qquad \text{and} \qquad \left\langle \mathbf{v}, \mathbf{w}\right\rangle_\gamma = \int_\gamma \mathbf{v} \cdot \mathbf{w} \, d\gamma \tag{8}$$

The Nitsche's statement equivalent to the problem in equation 2 is: Given the discrete subspace $V^h\left(\Omega\right) \subset H^1\left(\Omega\right)$, where H^1 is the space of piecewise continuous functions, find $u^h \in V^h\left(\Omega\right)$, such that $\forall w^h \in V^h\left(\Omega\right)$,

$$a^h\left(u^h, w^h\right) = l^h\left(w^h\right), \tag{9}$$

where

$$\begin{aligned} a^h\left(u^h, w^h\right) &= \left(\nabla w^h, \nabla u^h\right)_\Omega \\ &\quad - \left\langle w^h, \nabla u^h \cdot \mathbf{n}\right\rangle_{\Gamma_D} \\ &\quad - \left\langle \nabla w^h \cdot \mathbf{n}, u^h - u_D\right\rangle_{\Gamma_D} \\ &\quad + \left\langle \alpha / h^\perp w^h, u^h - u_D\right\rangle_{\Gamma_D}, \end{aligned} \tag{10}$$

$$l^h\left(w^h\right) = \left(w^h, f\right)_\Omega,$$

α is the penalization parameter, and $h^\perp$ the characteristic length, assumed as the maximum element height. The penalization parameter adopted for the first order elements used in this work is taken as $\alpha = 10$.

The shifted boundary statement is similarly defined. The same space is adopted for the approximation and weight functions, the same penalization parameter and characteristic length, the difference lying on the bilinear and linear functionals defined, with the help of the already defined parameters, as:

$$
\begin{aligned}
a^h\left(u^h, w^h\right) = &\left(\nabla w^h, \nabla u^h\right)_{\overline{\Omega}} \\
&- \left\langle w^h + \nabla w^h \cdot \mathbf{d}, \nabla u^h \cdot \widetilde{\mathbf{n}}\right\rangle_{\widetilde{\Gamma}_D} \\
&- \left\langle \nabla w^h \cdot \widetilde{\mathbf{n}}, u^h + \nabla u^h \cdot \mathbf{d}\right\rangle_{\widetilde{\Gamma}_D} \\
&+ \left\langle \nabla w^h \cdot \mathbf{d}, \left(\mathbf{n} \cdot \widetilde{\mathbf{n}}/||\mathbf{d}||\right) \nabla u^h \cdot \mathbf{d}\right\rangle_{\widetilde{\Gamma}_D} \\
&+ \left\langle \alpha/h^{\perp}\left(\nabla w^h + \nabla w^h \cdot \mathbf{d}\right), \nabla u^h + \nabla u^h \cdot \mathbf{d}\right\rangle_{\widetilde{\Gamma}_D}
\end{aligned}
\tag{11}
$$

$$
\begin{aligned}
l^h\left(w^h\right) = &\left(w^h, f\right)_{\overline{\Omega}} \\
&- \left\langle \nabla w^h \cdot \widetilde{\mathbf{n}}, \overline{u}_D\right\rangle_{\widetilde{\Gamma}_D} \\
&+ \left\langle \nabla w^h \cdot \mathbf{d}, \left(\nabla \overline{u}_D \cdot \tau_i\right) \tau_i \cdot \widetilde{\mathbf{n}}\right\rangle_{\widetilde{\Gamma}_D} \\
&+ \left\langle \alpha/h^{\perp}\left(\nabla w^h + \nabla w^h \cdot \mathbf{d}\right), \overline{u}_D\right\rangle_{\widetilde{\Gamma}_D} .
\end{aligned}
$$

The proved analytical convergence rate is of order 1.5, but the original publication also reports optimal second-order convergence rate, leaving open the speculation that the proved rate might be a lower boundary and liable to sharper estimations.

All implementation is performed using the c++ finite element framework called libMesh [14]. The framework aim is to serve as an infrastructure for mesh-based parallel adaptive algorithms. It provides all the infrastructure to quickly load data, assemble the discretized equation system, solve it by making usage of some third part supported linear algebra library, and write its output in the common open standard scientific data file. The framework has a diverse selection of finite element specific classes implemented, so the user can focus on the formulation or specific feature under scrutiny, making it a useful prototyping tool.

3 Results

For each of the two implemented formulations, Nitsche's and the Shifted Boundary, a set of six meshes is evaluated as the two-dimensional cases, and a set of five as three-dimensional cases, all of them with the same Dirichlet boundary condition, and both radius, inner and outer, are equals in all of the cases. This approach is aimed to homogenize the results just for convenience.

The meshes are increasingly denser so that the accuracy of the solution can be compared. The error evaluation is performed for the two-dimensional cases by projecting the analytical solution in the evaluated mesh, case by case. By doing this the comparison in performed into the same solution space available for the partition under evaluation, and have only error component perpendicular to this space.

The three dimensional cases evaluation were exploratory and do not have as an extensive evaluation as the two-dimensional ones. Nevertheless it is possible to compare the effect that a tighter partition has on the resulting field.

The parameters that defines both the annulus and spherical shell are:

$$
\begin{aligned}
f &= 0,\\
r_e &= 1,\\
r_i &= 0.5,\\
u_e &= 13,\\
u_i &= 34,
\end{aligned}
$$

where r_e is the external radius, r_i the inner radius, u_e the prescribed field in the external circle or sphere and u_i the prescribed field in the inner circle or sphere.

3.1 Annulus evaluation

For the conformal mesh the resulting scalar field can be seen in Figure 2. The mesh is not highlighted because in the denser case it would be impracticable to visualize the results, nevertheless increased resolution can be noted by the boundary shape. It is possible to notice the quick convergence to the expected field when in case 3 the element edge can not be visually distinguished.

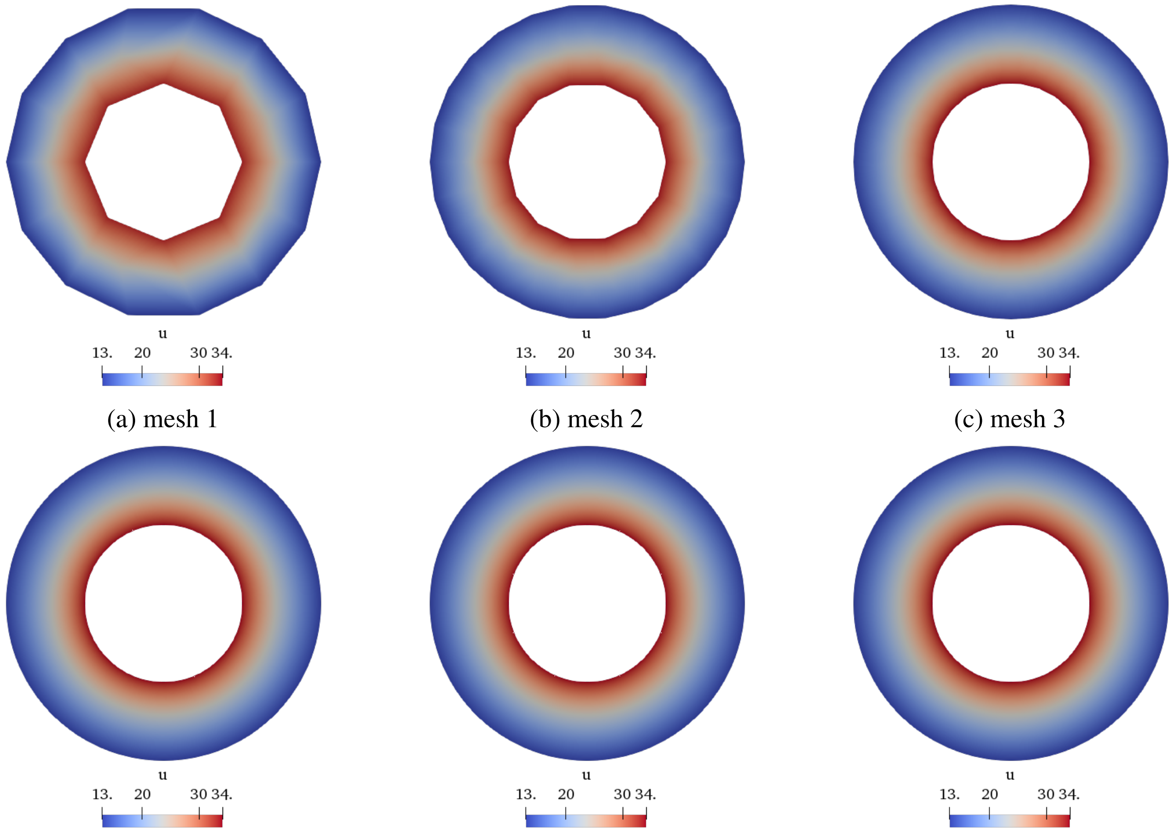

(a) mesh 1 (b) mesh 2 (c) mesh 3

(d) mesh 4 (e) mesh 5 (f) mesh 6

Figure 2. Resulting field for conformal formulation, annular domain.

The relative error evaluation, depicted in figure 3, was performed in the post processing phase, by applying the analytical solution as a nodal data, effectively representing its projection to the adopted mesh. As expected the error magnitude quickly diminishes and, as a relevant feature for comparison, one can note that it is homogeneously distributed through out the entire domain. The color scale is adjusted to the maximum and minimum value.

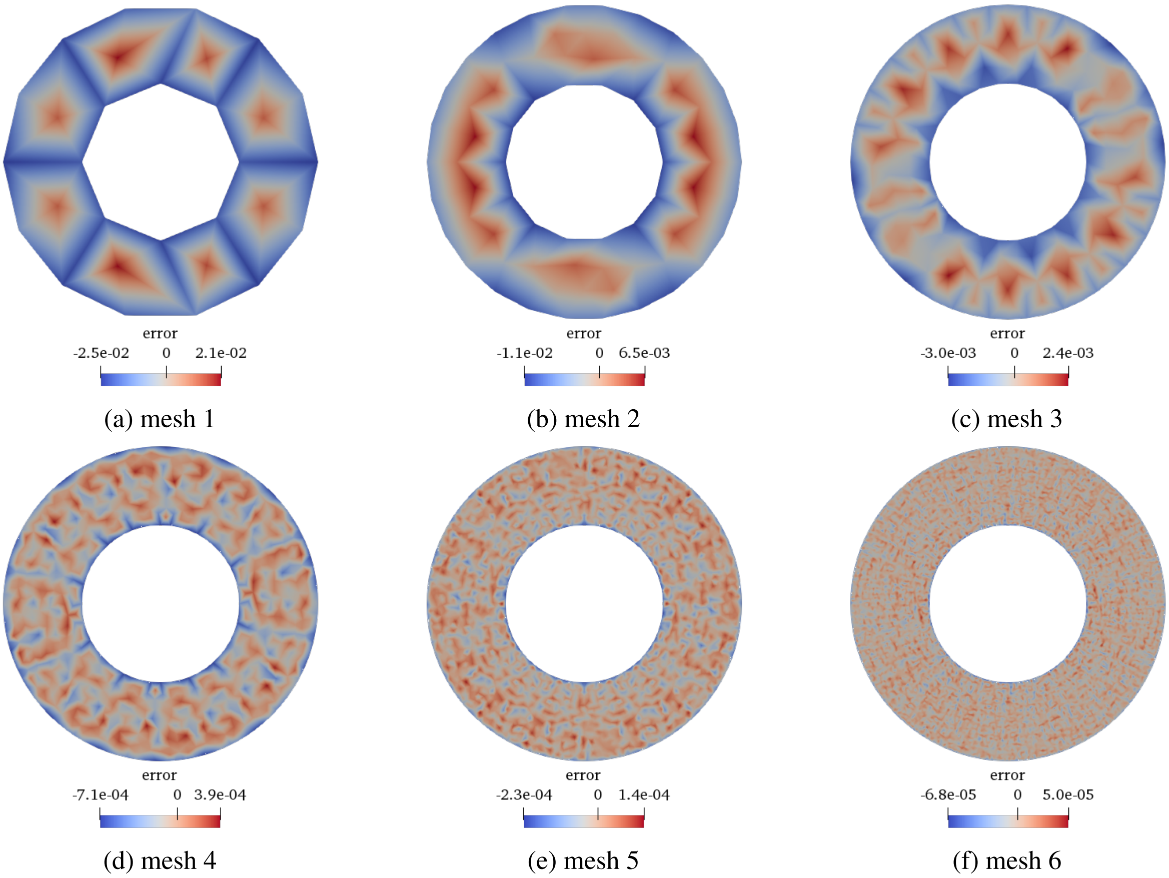

(a) mesh 1 (b) mesh 2 (c) mesh 3

(d) mesh 4 (e) mesh 5 (f) mesh 6

Figure 3. Relative error on conformal formulation, annular domain.

The subdomains for the first four meshes are depicted in figure 4. The red color indicates the elements crossed by the boundary, and so they are not considered, the yellow color indicates the surrogate boundary elements, and the dark blue color, the inner elements. The resulting domain depicted in the first mesh holds no resemblance with the intended geometry and is a remembrance that, though flexible, the embedded formulations still needs judicious examination.

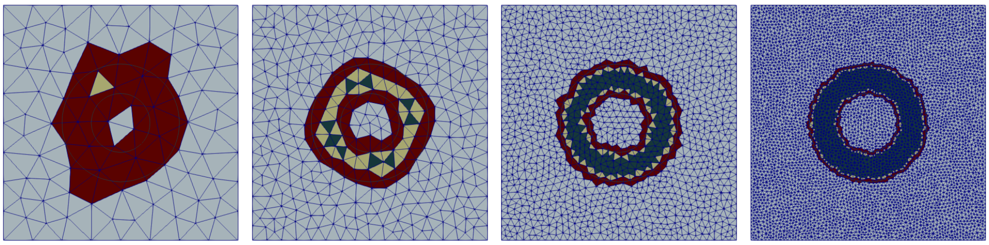

(a) mesh 1 (b) mesh 2 (c) mesh 3 (d) mesh 4

Figure 4. Subdomain evalution.

The resulting field for the surrogate boundary model is shown in figure 5. The jagged boundary approximates to a circle as the mesh gets denser. The resulting field is analogous to the conformal formulation and shows the right feature even on mesh 1, where it is possible to note the correct gradient direction. The asymptotic error lies in the chopped off region and is small as the distance between the true boundary and its surrogate. For this implementation the upper value for this distance is the maximum element size crossed by the boundary. The annulus outline is projected as reference.

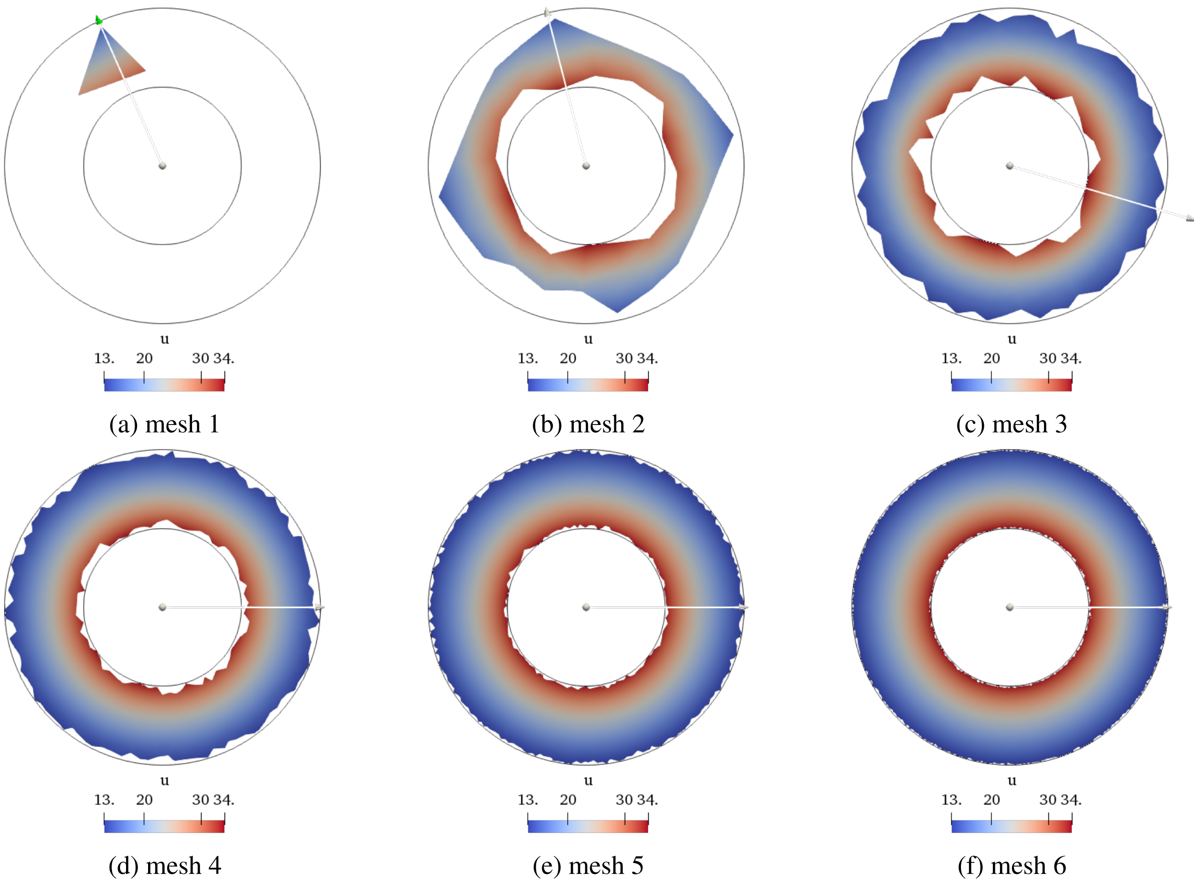

(a) mesh 1 (b) mesh 2 (c) mesh 3

(d) mesh 4 (e) mesh 5 (f) mesh 6

Figure 5. Surrogate formulation, annular domain.

Similarly to the conformal case, the relative error for the surrogate boundary formulation is evaluated taking as reference the analytical solution projected to the adopted mesh, and is show in figure 3, for all cases. The magnitude of the error diminishes down to 10^{-2} indicating its suitability. It is possible to note the different character of the error distribution, following the same annular shape and reaching higher values close to the boundaries. This indicates the error introduced by the surrogate boundary is dominant.

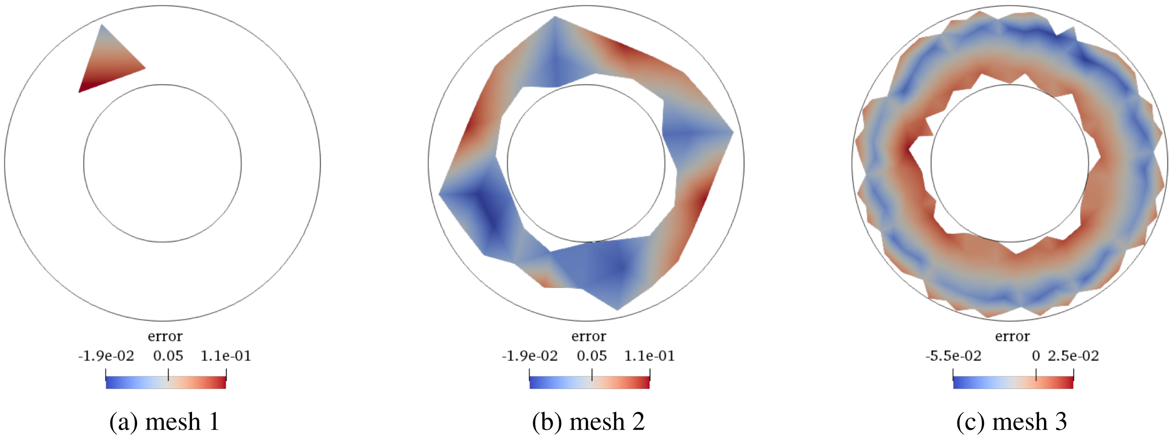

(a) mesh 1 (b) mesh 2 (c) mesh 3

Figure 6. Relative error on surrogate formulation, annular domain (continue).

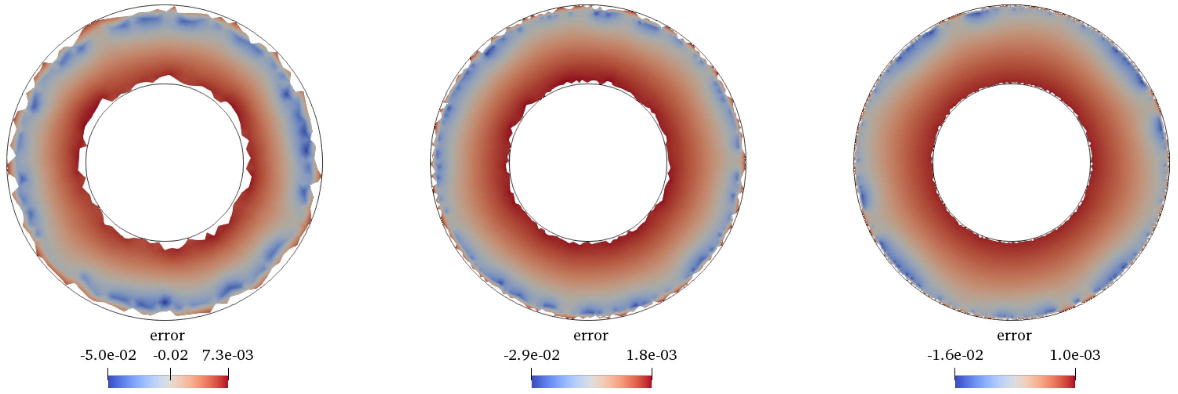

(d) mesh 4

(e) mesh 5

(f) mesh 6

Figure 6. Relative error on surrogate formulation, annular domain.

The plots depicted in figure 7 corresponds to field values sampled in the a radial direction for all the cases. The analytical curve plotted corresponds to its projection into the denser mesh, for each formulation. The arrows over the domains in figure 5 indicates sample line in the embedded cases. For the conformal cases it is not possible to distinguish the different curves from mesh 3 onward. The same feature is not as prominent for the surrogate boundary, and a greater deviation from the analytical solution occurs closer to the outer boundary.

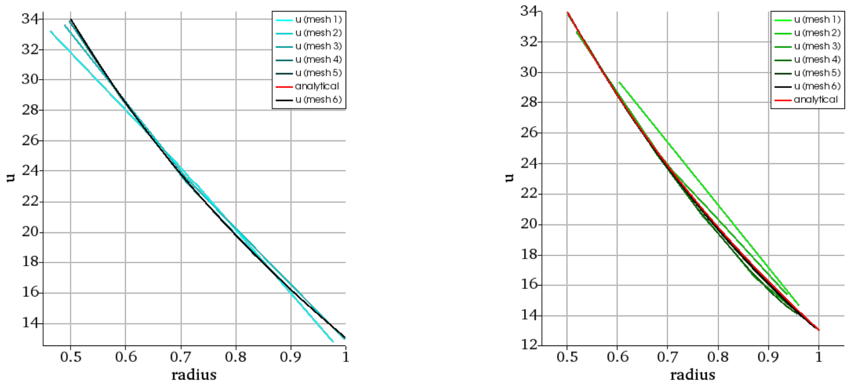

(a) Conformal

(b) Surrogate

Figure 7. Radial sampling of u on annular domain.

3.2 Spherical shell evaluation

For the spherical shell the five cases are also ordered according to the mesh density. Figure 8 displays the resulting field in a cuted section of the domain. It is possible to note the decreasing element size as the surface gets more spherical. The elements edges are not outlined for practical reasons as well. The resulting field displays a smooth aspect in all cases, indicating a good approximation.

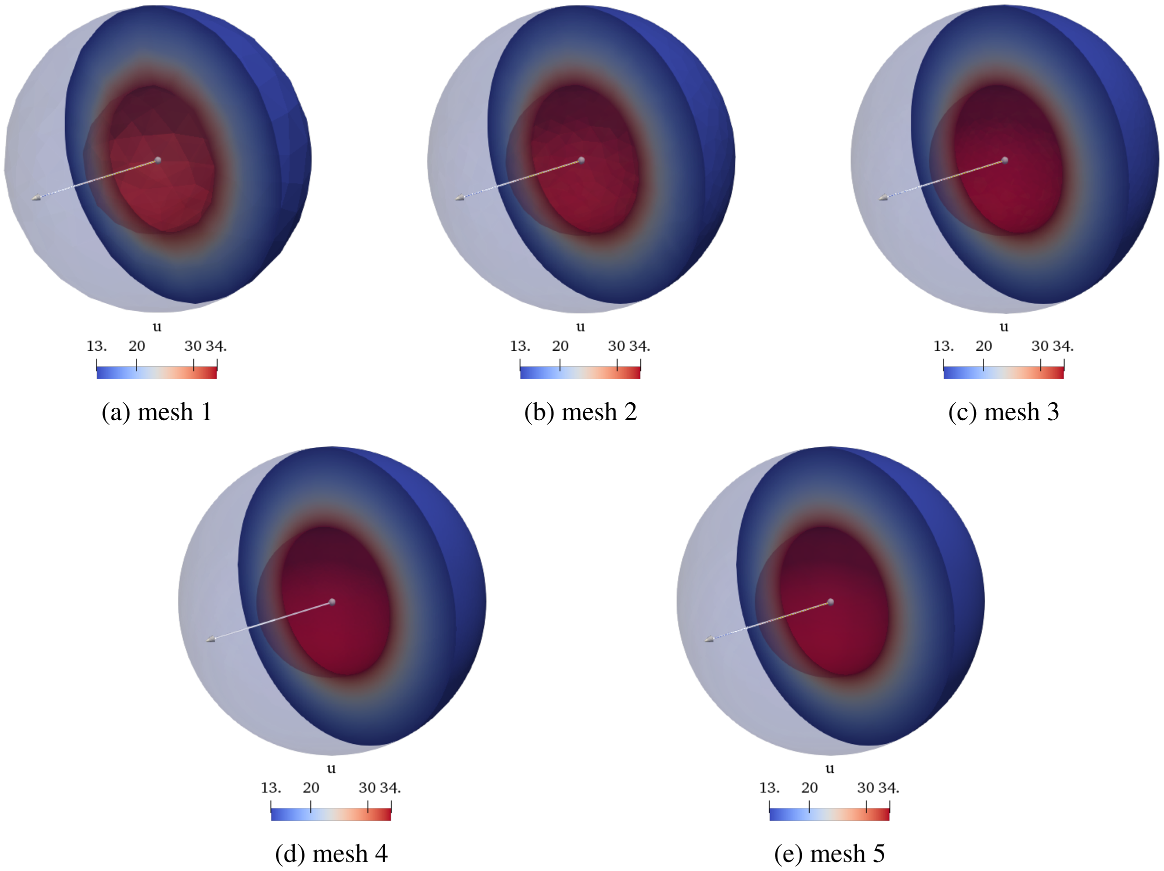

(a) mesh 1

(b) mesh 2

(c) mesh 3

(d) mesh 4

(e) mesh 5

Figure 8. Conformal formulation, spherical shell domain.

The resulting field for the surrogate model is show in figure 9. Mesh 1 is also too coarse and holds no resemblance to the intended geometry but, similarly to the annulus case, it shows the correct gradient direction. The displayed volumes are a half volume section of the already filtered surrogate and inner elements. Besides the chopped off region, the field aspect is increasingly alike the expected one.

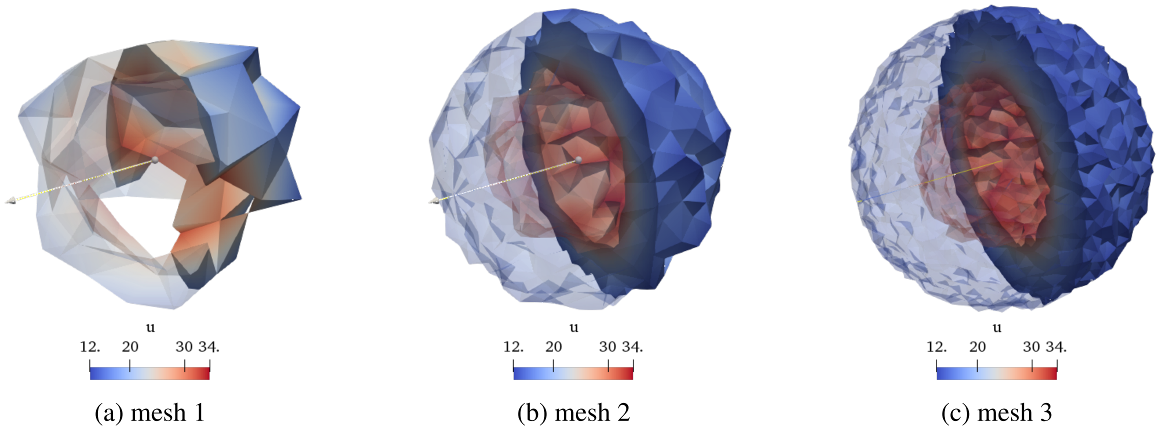

(a) mesh 1

(b) mesh 2

(c) mesh 3

Figure 9. Surrogate formulation, spherical shell domain (continue).

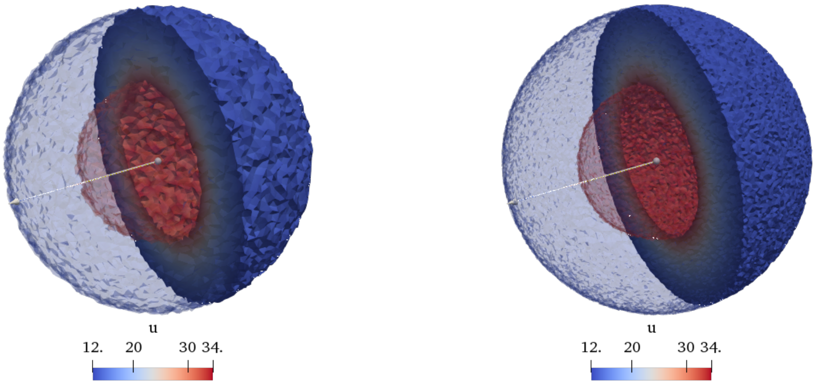

(d) mesh 4

(e) mesh 5

Figure 9. Surrogate formulation, spherical shell domain.

The plot depicted in figure 10 corresponds to field values sampled in the radial direction for all cases. For the conformal mesha quick a convergence to the reference value is also achieved, and it is not possible to distinguish the curves of mesh 3 and denser. The surrogate model shows a good enough approximation starting from mesh 3.

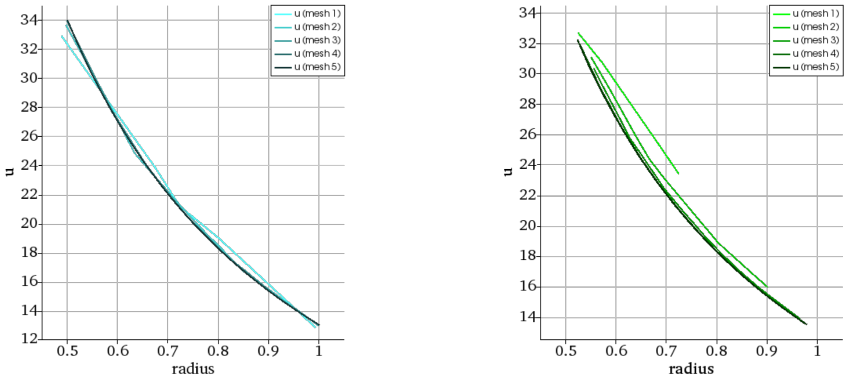

(a) conformal

(b) surrogate

Figure 10. Radial sampling of u on spherical shell domain.

4 Conclusion

The results indicates that the main source of error in the surrogate model is its boundary condition, and since its approximation is of first order, the smoothness of the field in the boundary neighborhood possibly plays a relevant role in the quality of the approximation. This conclusion is supported by the fact that, for the annulus error evaluation, a greater deviation from the analytical solution appeared closer to the outer boundary.

The surrogate boundary formulation is not suitable for evaluation of problems where the area of interest in the domain is close to the boundary, since that it is the probable chopped off region. This might be critical when evaluating the adoption of its siblings formulation [4] for other class of problems, like Stokes or Navier-Stokes equations. It might not be suitable for understanding boundary layers phenomena for instance, but probably relevant in simulations with interface problems.

Also the boundary distance can be arbitrarily small depending on the domain refinement region of choice. It is possible to purposely use meshes that are thinner close to the boundary, and so to control the average distance between the surrogate and the real one. On the limit this would bring back the issue of too much effort in mesh generation, with the additional cost of a lower order convergence. Part of this issue would be circumvent by adopting some adaptive mesh refinement criterion, but this approach could not be tested since in the current implementation libMesh cannot handle solution projections with subdomain-specific variables where elements are added to subdomains.

References

[Boggs et al.] Boggs, P. T., Althsuler, A., Larzelere, A. R., Walsh, E. J., Clay, R. L., & Hardwick, M. F. Dart system analysis.

[2] Cottrell, J., Hughes, T., & Bazilevs, Y., 2009. *Isogeometric Analysis: Toward Integration of CAD and FEA*. Wiley.

[3] Main, A. & Scovazzi, G., 2018a. The shifted boundary method for embedded domain computations. part i: Poisson and stokes problems. *Journal of Computational Physics*, vol. 372, pp. 972 – 995.

[4] Main, A. & Scovazzi, G., 2018b. The shifted boundary method for embedded domain computations. part ii: Linear advection–diffusion and incompressible navier–stokes equations. *Journal of Computational Physics*, vol. 372, pp. 996 – 1026.

[5] Peskin, C. S., 1972. Flow patterns around heart valves: A numerical method. *Journal of Computational Physics*, vol. 10, n. 2, pp. 252 – 271.

[6] Dunne, T., 2006. An eulerian approach to fluid–structure interaction and goal-oriented mesh adaptation. *International Journal for Numerical Methods in Fluids*, vol. 51, n. 9-10, pp. 1017–1039.

[7] Moës, N., Dolbow, J., & Belytschko, T., 1999. A finite element method for crack growth without remeshing. *International Journal for Numerical Methods in Engineering*, vol. 46, n. 1, pp. 131–150.

[8] Nitsche, J., 1971. Über ein variationsprinzip zur lösung von dirichlet-problemen bei verwendung von teilräumen, die keinen randbedingungen unterworfen sind. *Abhandlungen aus dem Mathematischen Seminar der Universität Hamburg*, vol. 36, n. 1, pp. 9–15.

[9] Hansbo, A. & Hansbo, P., 2002. An unfitted finite element method, based on nitsche's method, for elliptic interface problems. *Computer Methods in Applied Mechanics and Engineering*, vol. 191, n. 47, pp. 5537 – 5552.

[10] Schillinger, D., Düster, A., & Rank, E., 2012. The hp-d-adaptive finite cell method for geometrically nonlinear problems of solid mechanics. *International Journal for Numerical Methods in Engineering*, vol. 89, n. 9, pp. 1171–1202.

[11] Xu, F., Schillinger, D., Kamensky, D., Varduhn, V., Wang, C., & Hsu, M.-C., 2016. The tetrahedral finite cell method for fluids: Immersogeometric analysis of turbulent flow around complex geometries. *Computers & Fluids*, vol. 141, pp. 135 – 154. Advances in Fluid-Structure Interaction.

[12] Schillinger, D. & Ruess, M., 2015. The finite cell method: A review in the context of higher-order structural analysis of cad and image-based geometric models. *Archives of Computational Methods in Engineering*, vol. 22, n. 3, pp. 391–455.

[13] Hardwick, M. F., Clay, R. L., Boggs, P. T., Walsh, E. J., Larzelere, A. R., & Altshuler, A., 2005. Dart system analysis. Technical report, Sandia National laboratories.

[14] Kirk, B. S., Peterson, J. W., Stogner, R. H., & Carey, G. F., 2006. libmesh: a c++ library for parallel adaptive mesh refinement/coarsening simulations. *Engineering with Computers*, vol. 22, pp. 237–254.